Supporting Information

Electrodeposition of Cu on $NiCo_2O_4$ nanoarrays for efficient electrochemical nitrate reduction to ammonia

Chun Liu, [a] Shuxian Yang, [a] Yubin Xiang, [a] Liang Wang, *[b] Qin Tang, [c] Dongdong Zhu*[a]

[a] School of Chemistry and Materials Science, Jiangsu Key Laboratory of New Energy Devices and Interface Science, Nanjing University of Information Science & Technology, Nanjing, 210044 China. E-mail: dd.zhu@nuist.edu.cn

[b] Centre for Catalysis and Clean Energy, Griffith University, Gold Coast Campus, Gold Coast, Queensland 4222, Australia. E-mail: liang.wang@griffith.edu.au

[c] School of Chemistry and Chemical Engineering, Yancheng Institute of Technology, Yancheng, China

1 Experimental section

1.1 Materials

Urea ($CO(NH_2)_2$), nickel nitrate hexahydrate ($Ni(NO_3)_2 \cdot 6H_2O$), sodium citrate ($C_6H_5O_7Na_3$), salicylic acid ($C_7H_6O_3$), sodium nitroferricyanide dihydrate ($C_5FeN_6Na_2O \cdot 2H_2O$), and phosphoric acid ($H_3PO_4$) were purchased from Aladdin Ltd. (Shanghai, China). Potassium hydroxide (KOH), ammonium chloride (NH_4Cl), sulfanilamide ($C_6H_8N_2O_2S$), N-(1-naphthyl) ethylenediamine dihydrochloride ($C_{12}H_{14}N_2 \cdot 2HCl$), and Sodium hypochlorite (NaClO) were purchased from Macklin Inc. (Shanghai, China). Ammonium fluoride (NH_4F), cobalt(II) nitrate hexahydrate ($Co(NO_3)_2 \cdot 6H_2O$), ethanol absolute (C_2H_5OH), copper(II) sulfate pentahydrate ($CuSO_4 \cdot 5H_2O$), boric acid (H_3BO_3), sodium pyrophosphate tetrabasic decahydrate ($Na_4P_2O_7 \cdot 10H_2O$), potassium nitrate (KNO_3), hydrogen peroxide aqueous solution (H_2O_2), hydrochloric acid (HCl), sulfuric acid (H_2SO_4), and sodium hydroxide (NaOH) were purchased from China National Pharmaceutical Group Corp. (China). All reagents in this work were used without further purification. Ultrapure water (Millipore Milli-Q grade) with a resistivity of 18.25 MΩ was used in all experiments.

1.2 Preparation of Cu-$NiCo_2O_4$, $NiCo_2O_4$, and Cu

In brief, a piece of Ni foam (2 cm × 3 cm) was ultrasonicated in 2.0 M hydrochloric acid, ethanol absolute, and Milli-Q water for 8 min, respectively. Firstly, 2.0 mmol of $Ni(NO_3)_2 \cdot 6H_2O$, 4.0 mmol of $Co(NO_3)_2 \cdot 6H_2O$, 5.0 mmol of NH_4F and 12.0 mmol of urea were dissolved in 35.0 mL of Milli-Q water to form a transparent solution by magnetic stirring. Then the solution was transferred to a 50 mL Teflon-lined stainless-steel autoclave in which a piece of Ni foam was immersed into it. The autoclave was sealed and maintained at 120°C for 6 h in an electric oven. After the autoclave cooled down to room temperature, the NiCo-precursor was taken out and washed with water and ethanol several times, followed by drying at 60°C for 12 h. Secondly, $NiCo_2O_4$ was prepared by annealing NiCo-precursor at 450°C in air for 2 h. Finally, the electrolyte contained 22.0 mmol of $Na_4P_2O_7 \cdot 10H_2O$, 22.0 mmol of NH_4Cl, 2.5 mmol of $CuSO_4 \cdot 5H_2O$, and 60mL of 0.1 M boric acid solution. Cu was then introduced by electrodeposition using $NiCo_2O_4$ as the substrate at a current density of 2.5 A/cm^2 in the electrolyte for 240 s. Additionally, the plating solution was stirred at 500 rpm during the reaction. The Ag/AgCl electrode and platinum sheet were used as reference and counter electrodes, respectively. The resulting electrode was rinsed with deionized water and dried overnight in a vacuum drying oven to obtain Cu-$NiCo_2O_4$. For comparison, $NiCo_2O_4$ was synthesized similar to that of Cu-$NiCo_2O_4$ without the step of introducing Cu by electrodeposition. Cu was electrodeposited on Ni foam at a current density of 2.5 A/cm^2 in the electrolyte for 240 s.

1.3 Characterizations

The X-ray diffraction (XRD) patterns of the samples were obtained on Rigaku MiniFlex 600 with Cu Kα radiation. The morphology of the samples was characterized by field emission scanning electron microscopy (FESEM, Zeiss Gemini SEM 300) equipped with an energy dispersive spectrometer (EDS) and transmission electron microscopy (TEM, JEOL JEM-2100F). X-ray photoelectron spectroscopy (XPS) measurements were carried out on an ESCALab250 using Al Kα radiation, and the working voltage is 12.5 KV. The binding energy was calibrated to the C 1s peak of 284.8 eV.

1.4 Electrochemical measurements

All electrochemical measurements reported in this study were performed on a CHI 760E electrochemical workstation (Chenhua, Shanghai). The electrocatalytic performance of the obtained catalyst was evaluated by using a two-chamber H-type cell with a three-electrode system in which the cathode chamber was separated from the anode chamber through a cation exchange membrane (Nafion 117). The Nafion 117 was pretreated according to the reported literature (*Nat. Commun.*, 2025, **16**, 3774). The prepared electrode was used as the cathode, while Pt sheet and Hg/HgO electrode served as the counter and reference electrodes, respectively, and 1.0 M KOH solution (40 mL) containing 0.1 M KNO_3 was used as electrolyte. The linear sweep voltammetry (LSV) was performed at a scan rate of 10 mV s^{-1}. All potentials were recorded against the reversible hydrogen electrode (RHE), and no IR correction was applied for the presented results. The potentiostatic test was carried out at different potentials for 1.0 h with a stirring rate of 1000 rpm.

1.5 Detection of ammonia

The NH_3 concentration was determined by indophenol blue spectrophotometry. Under alkaline conditions, ammonia nitrogen (NH_3/NH_4^+) reacts with sodium hypochlorite (NaClO) and phenolic compounds (phenol or salicylic acid) to produce the blue color indophenol blue in the presence of a sodium nitroferricyanide dihydrate catalyst. Firstly, 2.5 g of sodium citrate and 2.5 g of salicylic acid were dissolved in 50.0 mL of 1.0 M NaOH to prepare the colorant, noted as Reagent A. Reagent B was 0.05 M NaClO. Dissolve 0.2 g of sodium nitroferricyanide dihydrate in 20 mL of ultrapure water to prepare the catalyst, noted as Reagent C. Secondly, the quantification process is as follows: take out a certain amount of electrolyte and dilute it to the detection range. Then take 2 mL of the diluted solution and add 2.0 mL of reagent A, 1.0 mL of reagent B and 0.2 mL of reagent C in turn, shake well to mix, and leave it for 2 hours away from light. Next, the UV-Vis absorbance was measured at a wavelength of 655 nm. The concentration-absorbance curve was calibrated using the standard NH_4Cl solution with concentrations of 0, 0.50, 1.00, 1.50, 2.00, and 2.50 ppm of 1.0 M KOH solution. Then the concentration of NH_3 product was calculated according to the absorbance and standard curve.

1.6 Detection of nitrite

The NO_2^- concentration was detected by the naphthalene ethylenediamine hydrochloride method. Under acidic conditions, nitrite will undergo diazotization with sulfanilamide, and then couple with N-(1-naphthyl) ethylenediamine dihydrochloride to form a rose-red azo dye. According to the intensity of its color, it is quantitatively determined by the spectrophotometric method. Firstly, 0.2 g N-(1-naphthyl) ethylenediamine dihydrochloride and 4.0 g sulfanilamide were dissolved in 50 mL of deionized water, to which 10 mL of phosphoric acid (ρ=1.7 g/mL) was added to obtain a mixed solution. Secondly, the quantification process is as follows: the electrolyte sample was collected and diluted to the detection range. Then 40 μl of the color reagent was added into the 2.0 ml sample solution, mixed thoroughly and rested for 20min at ambient conditions. Next, the UV-Vis absorbance was measured at a wavelength of 540 nm. The concentration-absorbance curve was calibrated using the standard KNO_2 solution with concentrations of 0, 0.20, 0.50, 1.00, 1.50, and 2.00 ppm of 1.0 M KOH solution. Then the concentration of NO_2^- product was calculated according to the absorbance and standard curve.

1.7 Calculations of faradaic efficiency (FE) and NH_3 yield

NH_3 FE = $(8 \times F \times V \times C \times A) / (M_{NH_3} \times Q) \times 100\%$

NO_2^- FE = $(2 \times F \times V \times C \times A) / (M_{NO_2^-} \times Q) \times 100\%$

NH_3 yield = $(C \times V \times A) / (M_{NH_3} \times S \times t)$

Where F is the Faraday constant (96485 C mol^{-1}), V is the volume of electrolyte in the H-cell cathode chamber (40 mL), C is the measured concentration of the diluted product, A is the dilution factor, M_{NH_3} is the molar mass of NH_3, $M_{NO_2^-}$ is the molar mass of NO_2^-, Q is the total quantity of applied electricity, S is the loaded area of catalyst (0.5 cm × 0.5 cm), t is the electrolysis time (1.0 h).

2 Supplementary Figures and Table

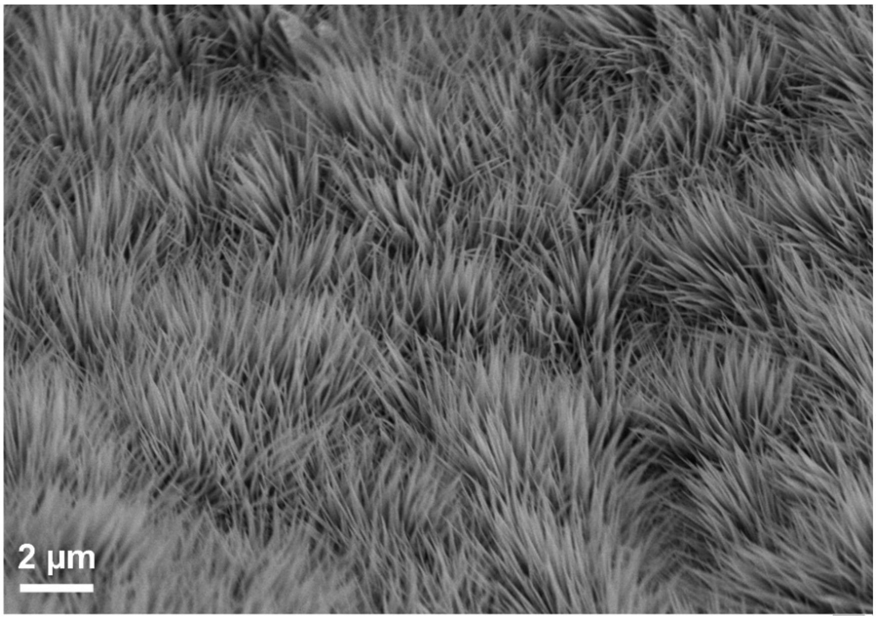

Figure S1. SEM image of NiCo-precursor.

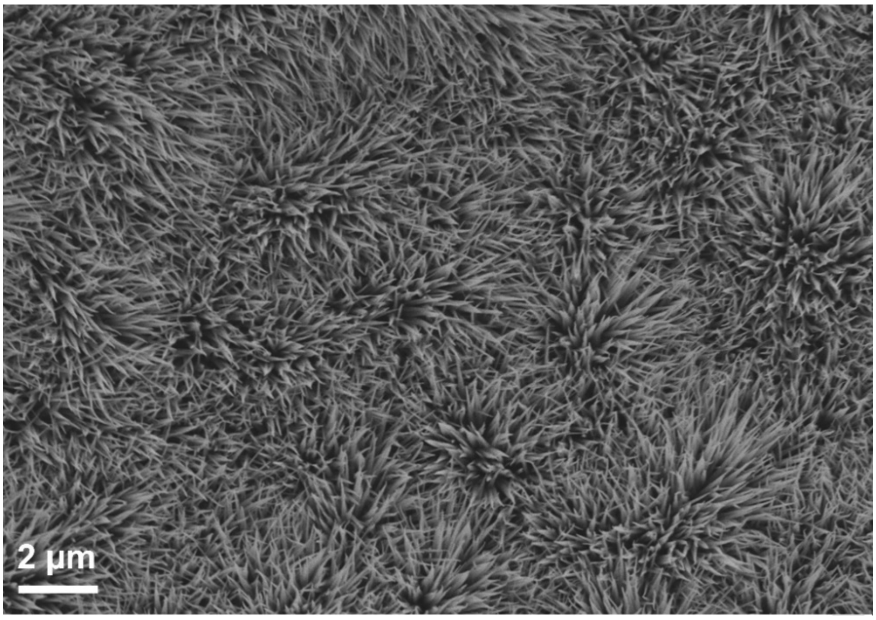

Figure S2. SEM image of $NiCo_2O_4$.

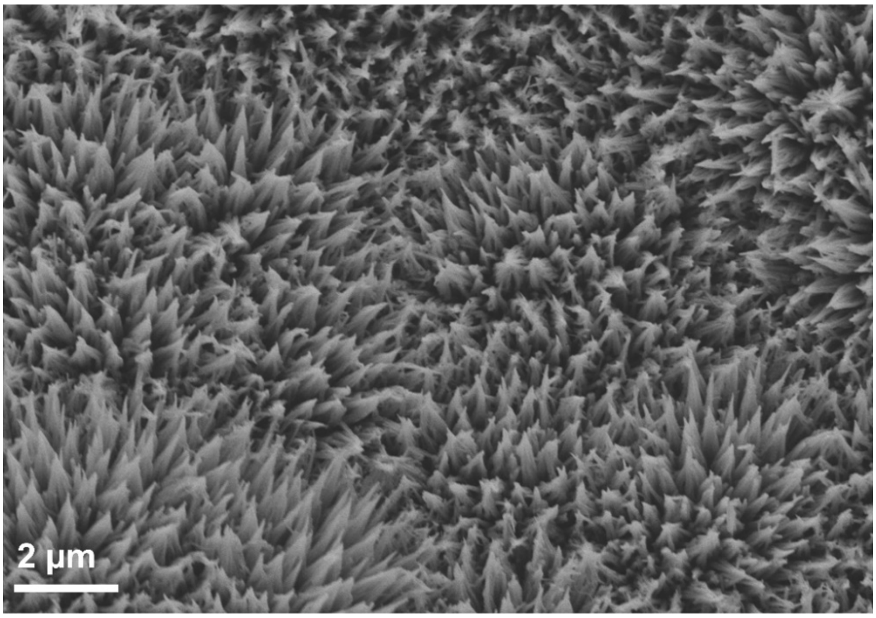

Figure S3. SEM image of Cu-$NiCo_2O_4$.

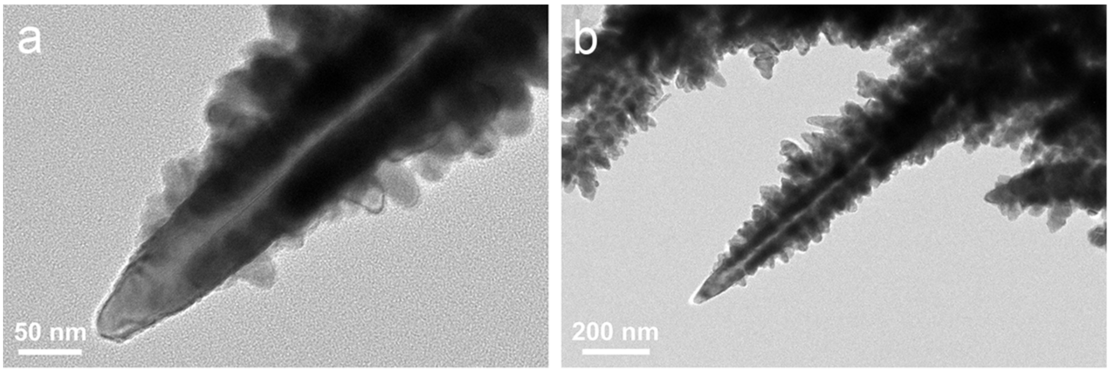

Figure S4. TEM images of Cu-$NiCo_2O_4$ with different resolutions.

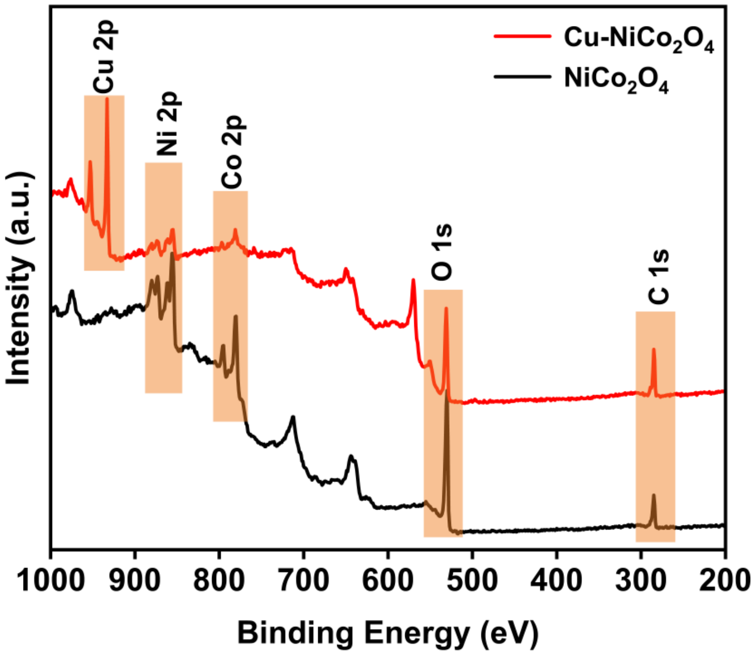

Figure S5. XPS survey spectra of Cu-NiCo$_2$O$_4$ and NiCo$_2$O$_4$.

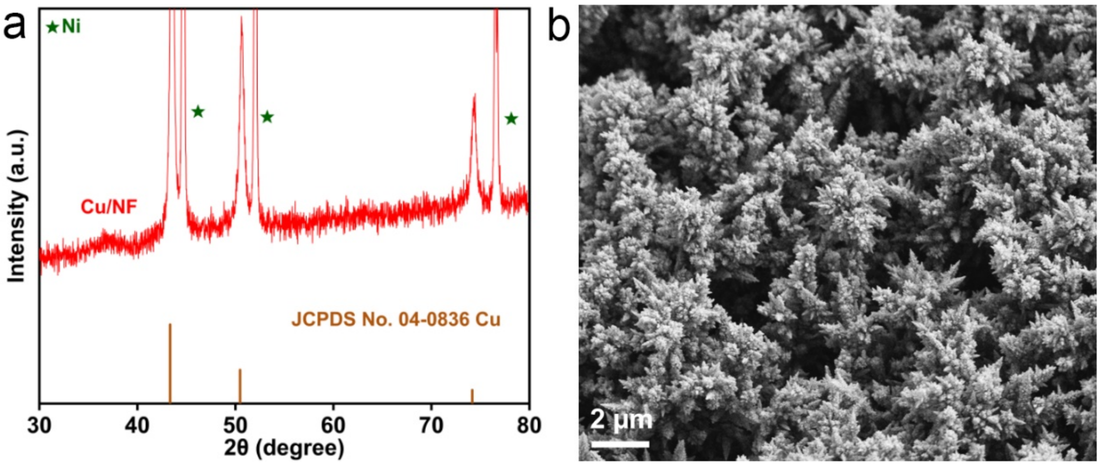

Figure S6. (a) XRD pattern of Cu/NF, and (b) SEM image Cu/NF.

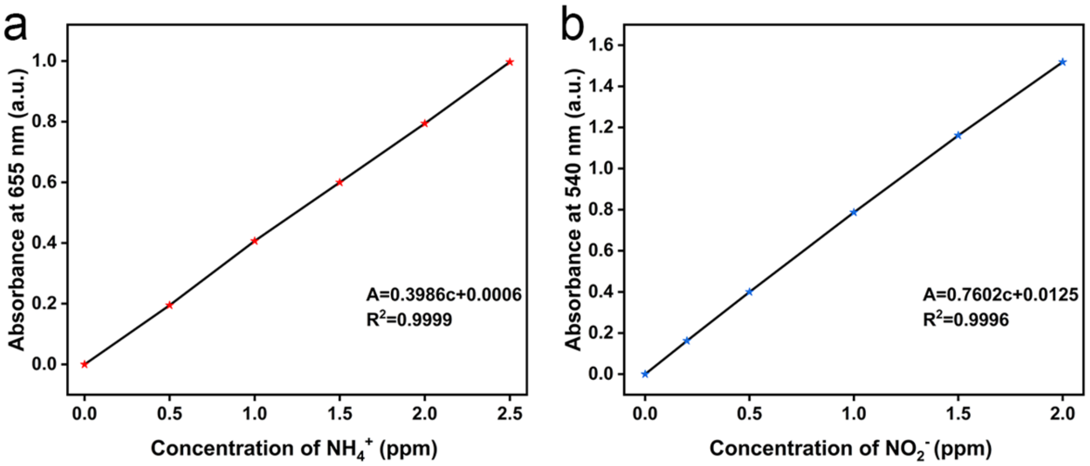

Figure S7. The concentration-absorbance calibration curves for (a) NH_4^+, and (b) NO_2^-.

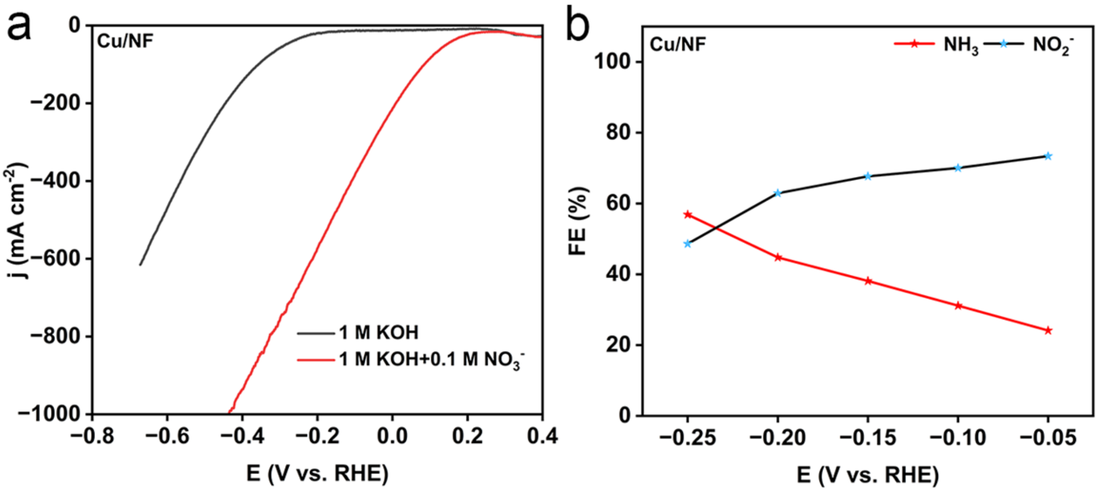

Figure S8. (a) LSV curves of Cu/NF in different electrolytes. (b) FEs of NH_3, and NO_2^- for Cu/NF at different applied potentials.

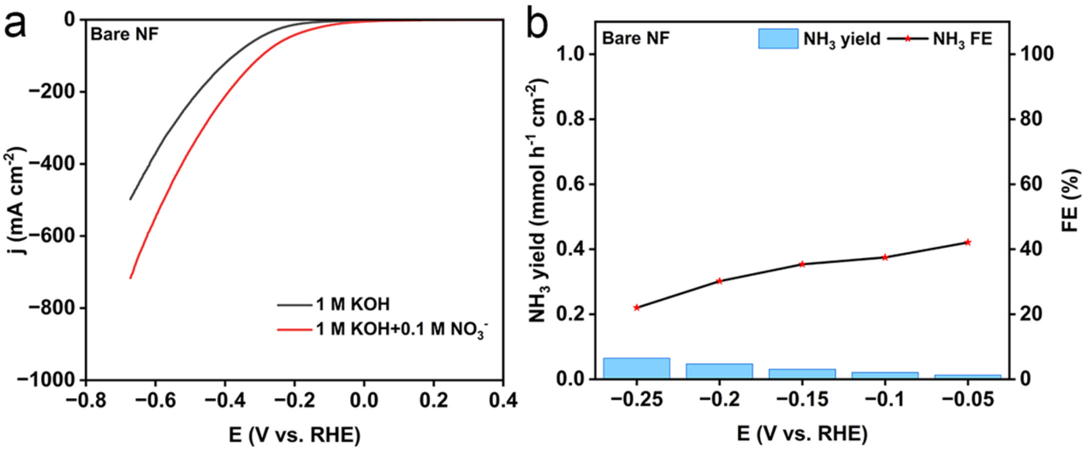

Figure S9. (a) LSV curves of bare NF in different electrolytes. (b) NH_3 yields and FEs of bare NF at different applied potentials.

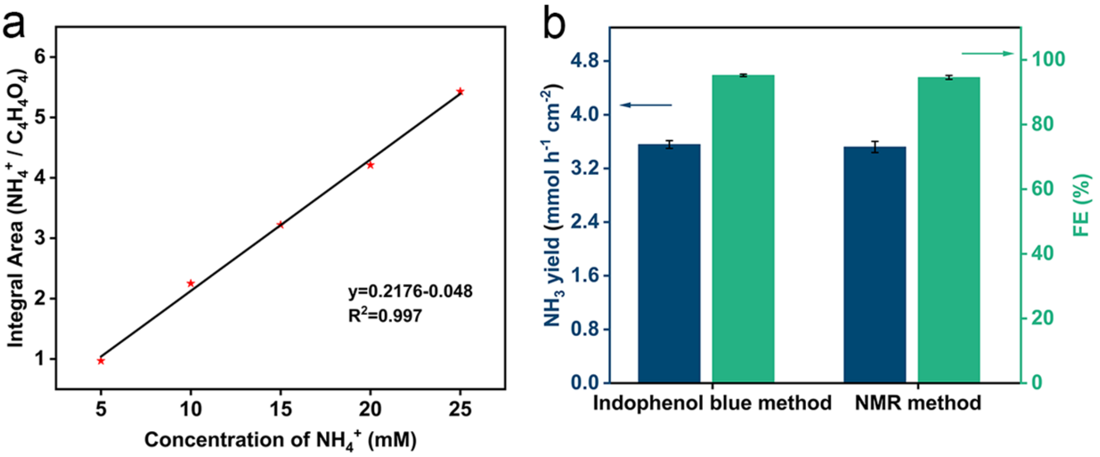

Figure S10. ^{1}H NMR analysis for the quantitative of ammonia. (a) The concentration–peak area calibration curves for NH_4^+. (b) NH_3 yields and FEs detected by NMR method and the indophenol blue method at −0.2 V *vs*. RHE.

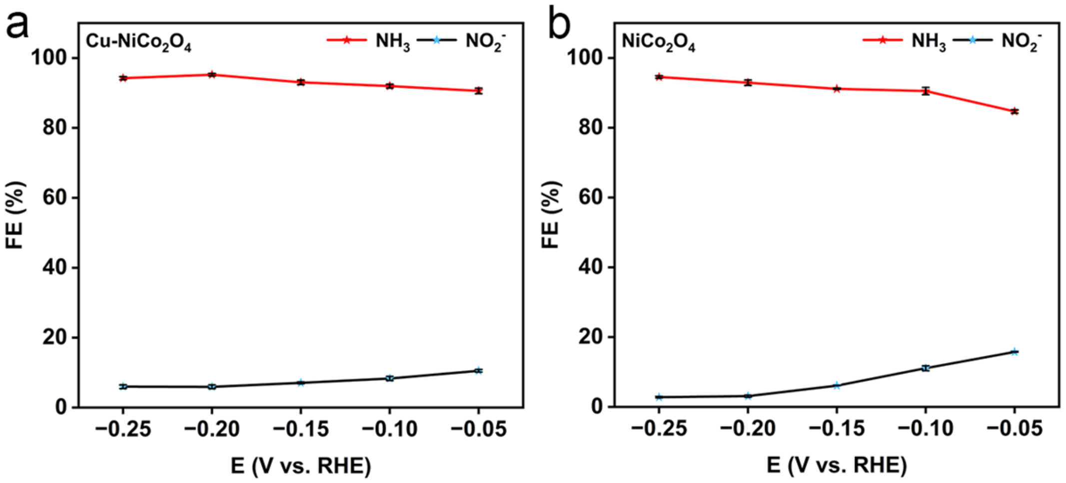

Figure S11. (a) FEs of NH_3, and NO_2^- for Cu-$NiCo_2O_4$ at different applied potentials. (b) FEs of NH_3, and NO_2^- for $NiCo_2O_4$ at different applied potentials.

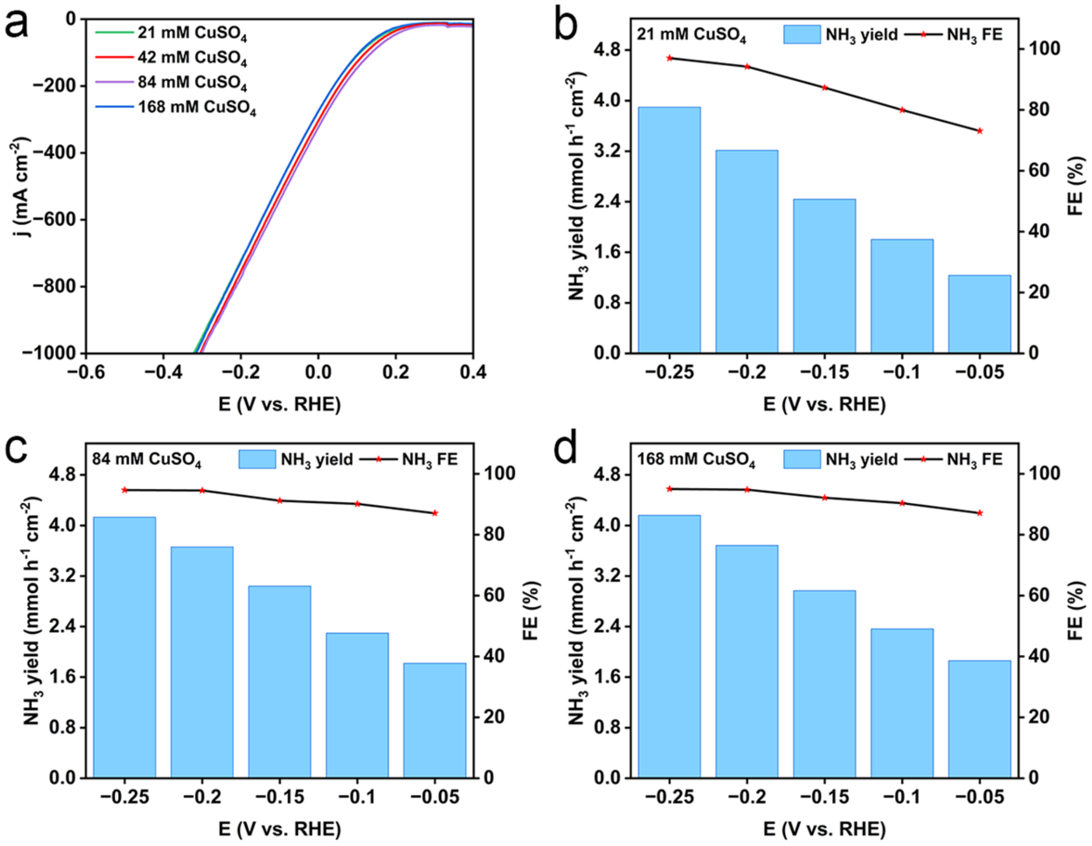

Figure S12. In 1.0 M KOH with 0.1 M NO_3^-, NO_3RR performance of Cu-$NiCo_2O_4$ samples prepared with different Cu content in the electrodeposition solution. (a) LSV curves of Cu-$NiCo_2O_4$ samples, (b) NH_3 yields and FEs of Cu-$NiCo_2O_4$ sample prepared with 21 mM $CuSO_4$ in the electrodeposition solution, (c) NH_3 yields and FEs of Cu-$NiCo_2O_4$ sample prepared with 84 mM $CuSO_4$ in the electrodeposition solution, and (d) NH_3 yields and FEs of Cu-$NiCo_2O_4$ sample prepared with 168 mM $CuSO_4$ in the electrodeposition solution.

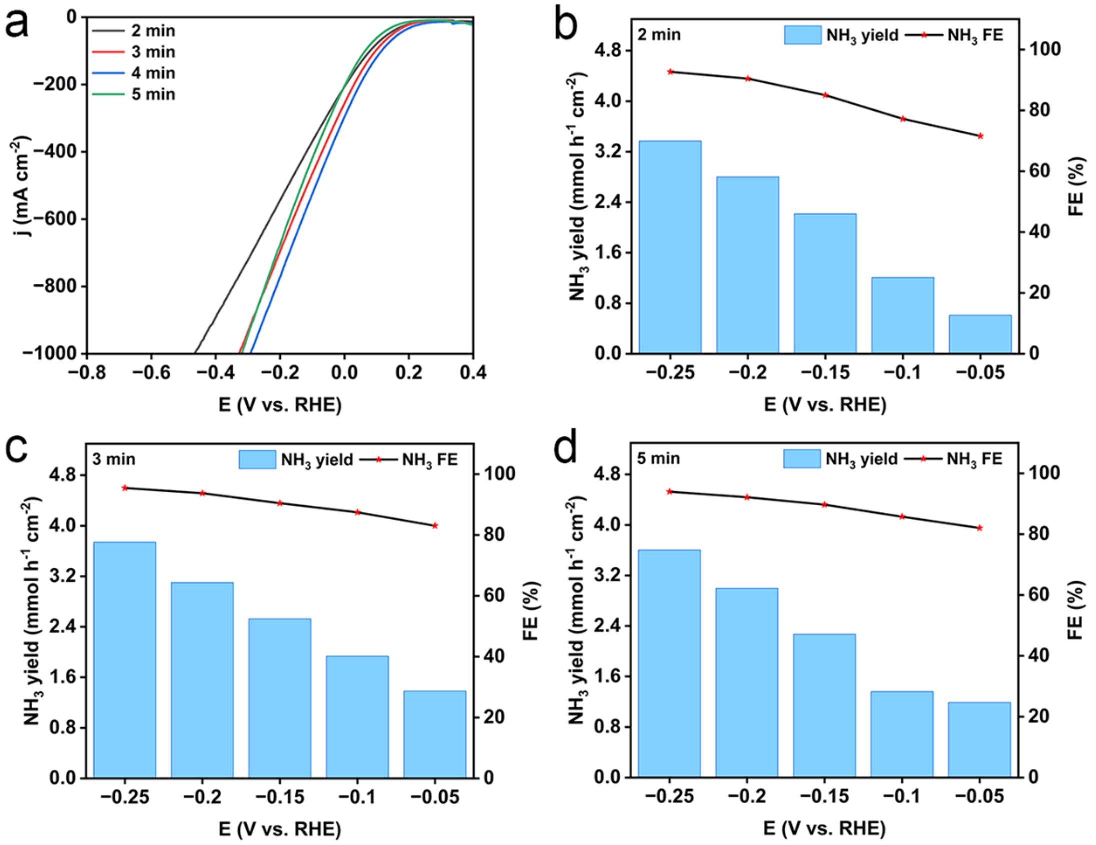

Figure S13. In 1.0 M KOH with 0.1 M NO_3^-, NO_3RR performance of Cu-$NiCo_2O_4$ samples prepared with different electrodeposition time. (a) LSV curves of Cu-$NiCo_2O_4$ samples, (b) NH_3 yields and FEs of Cu-$NiCo_2O_4$ sample prepared with 2 min, (c) NH_3 yields and FEs of Cu-$NiCo_2O_4$ sample prepared with 3 min, and (d) NH_3 yields and FEs of Cu-$NiCo_2O_4$ sample prepared with 5 min.

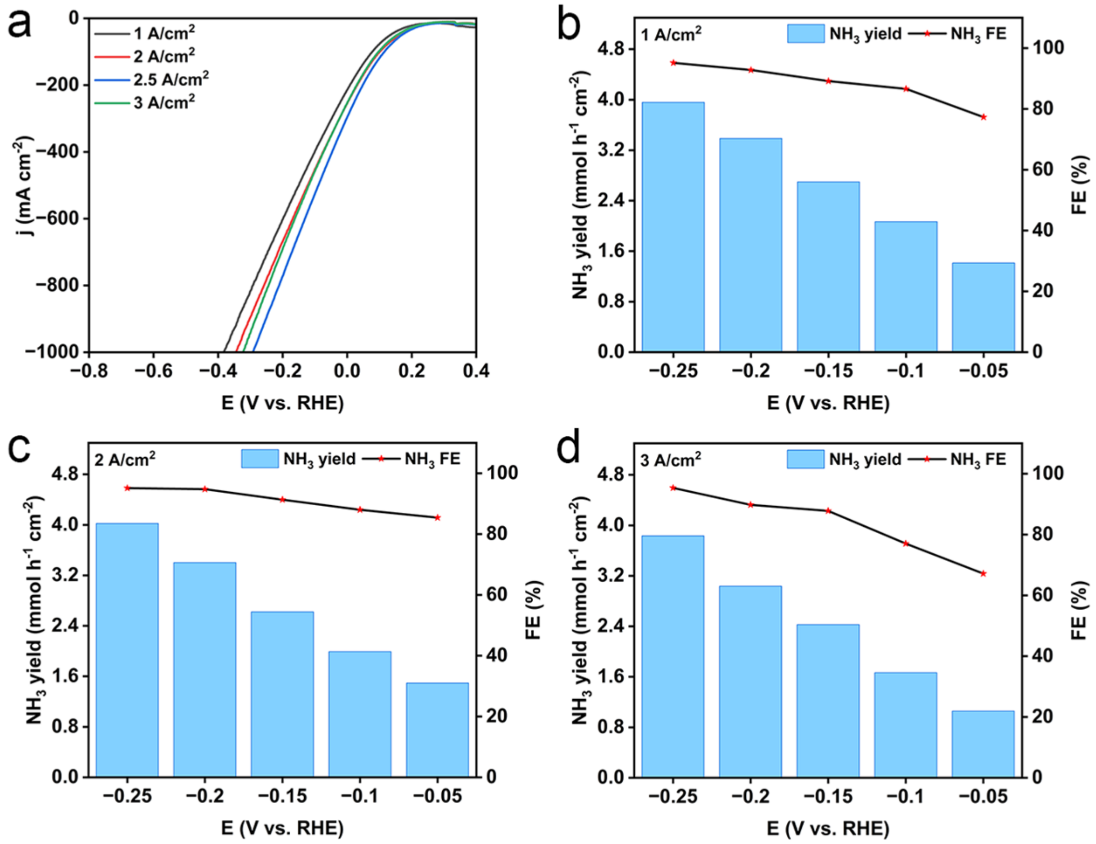

Figure S14. In 1.0 M KOH with 0.1 M NO_3^-, NO_3RR performance of Cu-$NiCo_2O_4$ samples prepared with different electrodeposition current density. (a) LSV curves of Cu-$NiCo_2O_4$ samples, (b) NH_3 yields and FEs of Cu-$NiCo_2O_4$ sample prepared with 1 A/cm^2, (c) NH_3 yields and FEs of Cu-$NiCo_2O_4$ sample prepared with 2 A/cm^2, and (d) NH_3 yields and FEs of Cu-$NiCo_2O_4$ sample prepared with 3 A/cm^2.

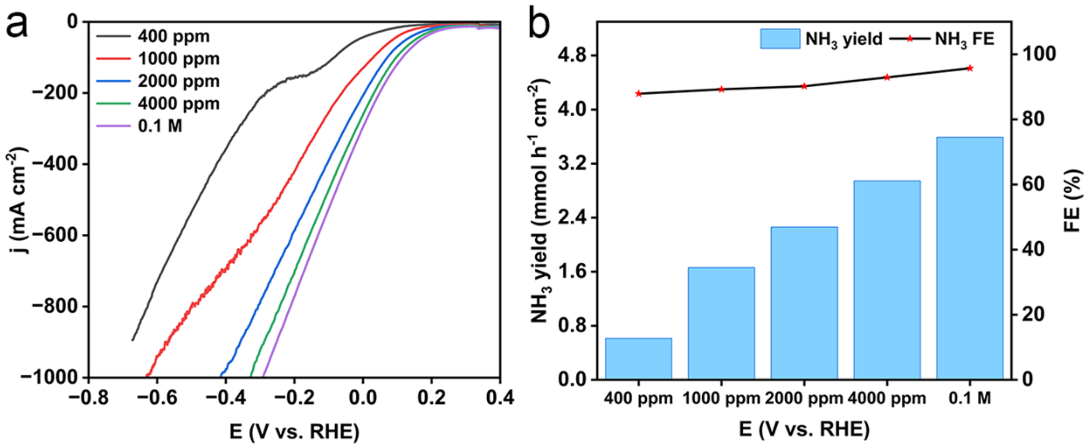

Figure S15. (a) LSV curves of Cu-$NiCo_2O_4$ tested in 1.0 M KOH with different NO_3^- concentrations. (b) NH_3 yields and FEs of Cu-$NiCo_2O_4$ tested at −0.2 V *vs.* RHE in 1.0 M KOH with different NO_3^- concentrations.

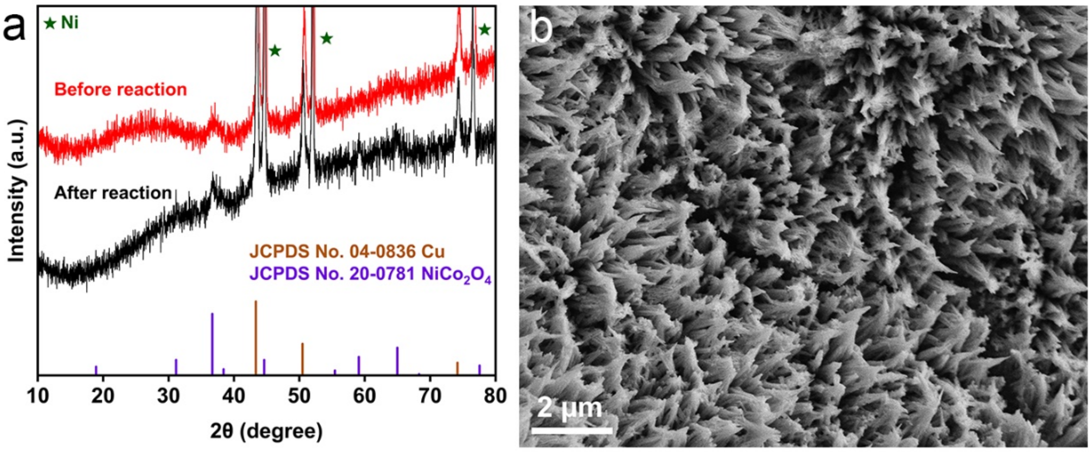

Figure S16. (a) XRD patterns of Cu-$NiCo_2O_4$ before and after NO_3RR cycling test. (b) SEM image of Cu-$NiCo_2O_4$ after NO_3RR cycling test.

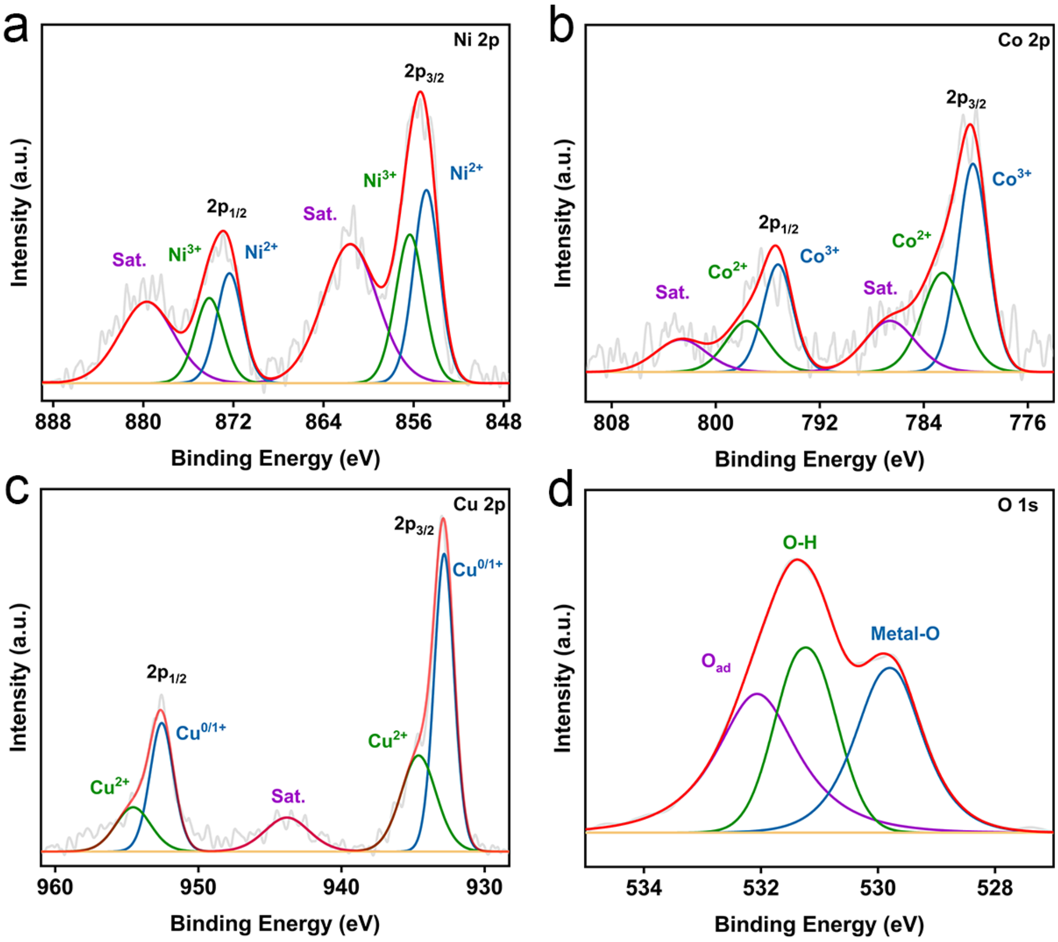

Figure S17. XPS spectra of Cu-$NiCo_2O_4$ after the stability test: (a) Ni 2p, (b) Co 2p, (c) Cu 2p, and (d) O 1s.

Table S1. Summary of the UV-vis absorption data of diluted electrolytes after NO_3RR for $Cu\text{-}NiCo_2O_4$ and $NiCo_2O_4$ catalysts.

Catalyst	**Group**	**Potential (V *vs.* RHE)**	**Absorbance at 655 nm (a.u.)**
$Cu\text{-}NiCo_2O_4$	1	−0.25	0.733
		−0.2	0.631
		−0.15	0.548
		−0.1	0.432
		−0.05	0.331
	2	−0.25	0.72
		−0.2	0.621
		−0.15	0.518
		−0.1	0.411
		−0.05	0.329
	3	−0.25	0.711
		−0.2	0.611
		−0.15	0.515
		−0.1	0.409
		−0.05	0.326
$NiCo_2O_4$	1	−0.25	0.334
		−0.2	0.249
		−0.15	0.165
		−0.1	0.095
		−0.05	0.051
	2	−0.25	0.348
		−0.2	0.252
		−0.15	0.178
		−0.1	0.108
		−0.05	0.058
	3	−0.25	0.342
		−0.2	0.248
		−0.15	0.168
		−0.1	1.04
		−0.05	0.054

Table S2. Summary of the electrochemical NO_3RR performance of some representative electrocatalysts in alkaline electrolytes.

Catalyst	**Electrolyte**	**Potential (V vs. RHE)**	**NH_3 yield (mmol h^{-1} cm^{-2})**	**NH_3 FE (%)**	**Ref.**
Cu-$NiCo_2O_4$	1 M KOH + 0.1 M NO_3^-	−0.2	3.56	95.2	This work
NF/Ni_3N-Cu	1 M KOH + 0.1 M NO_3^-	−0.3	1.19	98.7	1
$NiCo_2O_4$	0.1 M NaOH + 0.1 M NO_3^-	−0.6	0.973	95.2	2
CuCo nanosheet	1 M KOH + 0.1 M NO_3^-	−0.2	4.8	90	3
CNS-CoP/CF	1 M KOH + 1 M NO_3^-	−1.03	8.47	88.6	4
Co/PN-C	1 M KOH + 0.1 M NO_3^-	−0.35	2.65	97.8	5
W-O-CoP	1 M KOH + 0.1 M NO_3^-	−0.5	4.76	95.2	6
NiCo LDH	1 M KOH + 32.3 mM NO_3^-	−0.214	2.35	94.25	7
Sn-FeS_2	1 M KOH + 0.1 M NO_3^-	−0.5	0.929	96.7	8
R-CoCu@CF	1 M KOH + 0.1 M NO_3^-	−0.5	3.9	97.7	9
$Cu_{50}Ni_{50}$ alloy	1 M KOH + 0.1 M NO_3^-	−0.15	0.42	99	10
CuNi-LDHs	0.1 M KOH + 0.1 M NO_3^-	−0.4	0.161	94.65	11
Co_3CuN	0.5 M KOH + 2000 ppm NO_3^-	−0.3	0.455	97	12
Ru-Cu NW	1 M KOH + 0.1 M NO_3^-	−0.135	4.5	96	13
Ru nanoclusters	1 M KOH + 1 M NO_3^-	−0.2	1.17	~100	14
PdCu	1 M KOH + 1 M NO_3^-	−0.2	1.25	92.5	15

References

1. X. Ouyang, W. Qiao, Y. Yang, B. Xi, Y. Yu, Y. Wu, J. Fang, P. Li and S. Xiong, *Angew. Chem. Int. Ed.*, 2025, **64**, e202422585.
2. Q. Liu, L. Xie, J. Liang, Y. Ren, Y. Wang, L. Zhang, L. Yue, T. Li, Y. Luo, N. Li, B. Tang, Y. Liu, S. Gao, A. A. Alshehri, I. Shakir, P. O. Agboola, Q. Kong, Q. Wang, D. Ma and X. Sun, *Small*, 2022, **18**, 2106961.
3. J.-Y. Fang, Q.-Z. Zheng, Y.-Y. Lou, K.-M. Zhao, S.-N. Hu, G. Li, O. Akdim, X.-Y. Huang and S.-G. Sun, *Nat. Commun.*, 2022, **13**, 7899.
4. K. Fan, W. Xie, J. Li, Y. Sun, P. Xu, Y. Tang, Z. Li and M. Shao, *Nat. Commun.*, 2022, **13**, 7958.
5. B. Yang, Y. Zhou, Z. Huang, B. Mei, Q. Kang, G. Chen, X. Liu, Z. Jiang, M. Liu and N. Zhang, *Nano Energy*, 2023, **117**, 108901.
6. Z. Chang, G. Meng, Y. Chen, C. Chen, S. Han, P. Wu, L. Zhu, H. Tian, F. Kong, M. Wang, X. Cui and J. Shi, *Adv. Mater.*, 2023, **35**, 2304508.
7. X. Zhang, X. Liu, Z.-F. Huang, L. Guo, L. Gan, S. Zhang, M. Ajmal, L. Pan, C. Shi, X. Zhang, G. Yang and J.-J. Zou, *ACS Catal.*, 2023, **13**, 14670−14679.
8. G. Zhang, F. Wang, K. Chen, J. Kang and K. Chu, *Adv. Funct. Mater.*, 2024, **34**, 2305372.
9. L. Qiao, A. Zhu, D. Liu, K. An, J. Feng, C. Liu, K. W. Ng and H. Pan, *Adv. Energy Mater.*, 2024, **14**, 2402805.
10. Y. Wang, A. Xu, Z. Wang, L. Huang, J. Li, F. Li, J. Wicks, M. Luo, D.-H. Nam, C.-S. Tan, Y. Ding, J. Wu, Y. Lum, C.-T. Dinh, D. Sinton, G. Zheng and E. H. Sargent, *J. Am. Chem. Soc.*, 2020, **142**, 5702−5708.
11. H. Li, S. Li, R. Guan, Z. Jin, D. Xiao, Y. Guo and P. Li, *ACS Catal.*, 2024, **14**, 12042−12050.
12. Z. Gong, X. Xiang, W. Zhong, C. Jia, P. Chen, N. Zhang, S. Zhao, W. Liu, Y. Chen and Z. Lin, *Angew. Chem. Int. Ed.*, 2023, **62**, e202308775.
13. F.-Y. Chen, Z.-Y. Wu, S. Gupta, D. J. Rivera, S. V. Lambeets, S. Pecaut, J. Y. T. Kim, P. Zhu, Y. Z. Finfrock, D. M. Meira, G. King, G. Gao, W. Xu, D. A. Cullen, H. Zhou, Y. Han, D. E. Perea, C. L. Muhich and H. Wang, *Nat. Nanotechnol.*, 2022, **17**, 759−767.
14. J. Li, G. Zhan, J. Yang, F. Quan, C. Mao, Y. Liu, B. Wang, F. Lei, L. Li, A. W. M. Chan, L. Xu, Y. Shi, Y. Du, W. Hao, P. K. Wong, J. Wang, S.-X. Dou, L. Zhang and J. C. Yu, *J. Am. Chem. Soc.*, 2020, **142**, 7036−7046.
15. H. Yin, Z. Chen, S. Xiong, J. Chen, C. Wang, R. Wang, Y. Kuwahara, J. Luo, H. Yamashita, Y. Peng and J. Li, *Chem Catal.*, 2021, **1**, 1088−1103.